Acta Crystallographica Section A
Foundations of Crystallography
ISSN 0108-7673

Received 23 September 2009
Accepted 25 November 2009

Tracking ligand-migration pathways of carbonmonoxy myoglobin in crystals at cryogenic temperatures

Ayana Tomita,[a,b] Tokushi Sato,[b,c] Shunsuke Nozawa,[b,c] Shin-ya Koshihara[a,b] and Shin-ichi Adachi[b,c]*

[a]Department of Materials Science, Tokyo Institute of Technology, Meguro, Tokyo 152-8551, Japan, [b]Non-equilibrium Dynamics Project, Exploratory Research for Advanced Technology (ERATO), Japan Science and Technology Agency (JST), Tsukuba, Ibaraki 305-0801, Japan, and [c]Photon Factory, High Energy Accelerator Research Organization (KEK), 1-1 Oho, Tsukuba, Ibaraki 305-0801, Japan. Correspondence e-mail: shinichi.adachi@kek.jp

In order to explore the ligand-migration dynamics in myoglobin induced by photodissociation, cryogenic X-ray crystallographic investigations of carbonmonoxy myoglobin crystals illuminated by continuous wave and pulsed lasers at 1–15 kHz repetition rate have been carried out. Here it is shown that this novel method, extended pulsed-laser pumping of carbonmonoxy myoglobin, promotes ligand migration in the protein matrix by crossing the glass transition temperature repeatedly, and enables the visualization of the migration pathway of the photodissociated ligands in native Mb at cryogenic temperatures. It has revealed that the migration of the CO molecule into each cavity induces structural changes of the amino-acid residues around the cavity which result in the expansion of the cavity. The sequential motion of the ligand and the cavity suggests a self-opening mechanism of the ligand-migration channel arising by induced fit.

1. Introduction

Proteins are not rigid but constantly fluctuating biomolecules. They must be fluctuating because they need to accommodate exogenous ligand molecules inside or on their surface to carry out their functions. Comprehensive understanding of the protein function requires knowledge of how the ligand molecules migrate to their binding sites through the protein matrix. A simple model system for studying this issue is myoglobin (Mb), a small globular heme protein that reversibly binds gaseous ligands at the heme iron site inside the protein matrix. Mb, often referred to as the hydrogen atom of biology and a paradigm of complexity, has played a central role in research on the photo-induced response of proteins and migration of gases, solvents and ligands in the protein matrix (Fenimore *et al.*, 2002). No open channel for accessing the docking site in myoglobin has been detected in its static X-ray structures, which shows that the fluctuation of the protein molecule is essential.

A number of time-resolved spectroscopic measurements of the Mb photoproduct have revealed a complex ligand-binding reaction with multiple kinetic intermediates (Austin *et al.*, 1975; Alben *et al.*, 1982; Henry *et al.*, 1983; Olson & Phillips, 1996; Scott & Gibson, 1997). After dissociation from the heme iron, ligands either rebind internally from the distal heme pocket or escape into the solvent. As no exit channel for the ligand molecule has been detected by X-ray crystallography, it is believed that the escape of the ligand is assisted by thermal fluctuations that transiently open exit channels. Lowering the temperature slows down the thermal fluctuations, and the internal binding process becomes dominant. Below the glass transition temperature around 180 K, large-scale protein fluctuations become arrested, so that ligands remain in the heme cavity after photodissociation.

This multiple kinetic scheme has motivated crystallographers to characterize structural features of the multiple intermediates by using both time-resolved crystallography (Šrajer *et al.*, 1996, 2001; Schotte *et al.*, 2003, 2004; Bourgeois *et al.*, 2003, 2006; Schmidt *et al.*, 2005) and cryogenic crystallography (Teng *et al.*, 1994, 1997; Schlichting *et al.*, 1994; Hartmann *et al.*, 1996; Vitkup *et al.*, 1997; Chu *et al.*, 2000; Ostermann *et al.*, 2000; Adachi *et al.*, 2003). The general picture from these experiments is that Mb has several internal cavities favorable for gas molecules to reside in, which are identified as Xe binding sites (Tilton *et al.*, 1984), as shown in Fig. 1. The gas ligands hop from one cavity to another *via* an unspecified mechanism, but it is generally agreed that the thermal fluctuation must play a role. However, the overall migration processes including the location and properties of the connections between the internal cavities as well as of the exit channels from Mb have not been fully characterized yet.

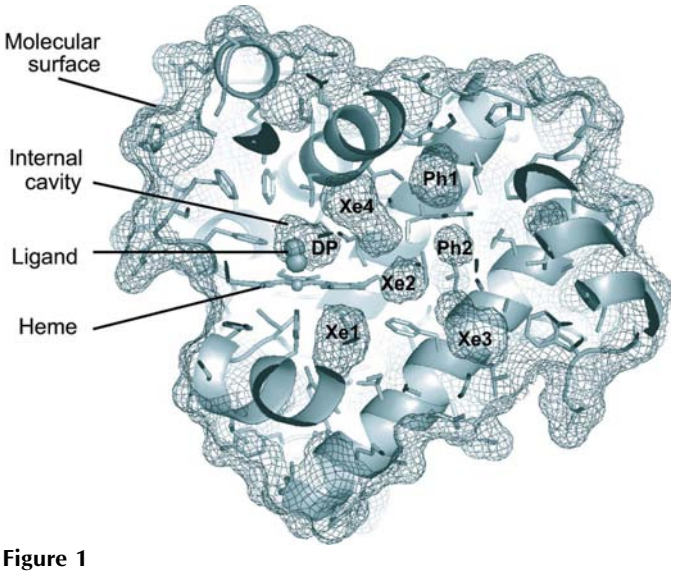

Figure 1
The crystal structure of carbonmonoxy myoglobin (MbCO). The molecular surface of MbCO and the surfaces of the internal cavities are shown by the mesh. The internal cavities labeled as the distal pocket (DP), Xe1, Xe2, Xe3, Xe4, Ph1 and Ph2 are also shown.

Mainly two types of experiment, 'time-resolved crystallography with pulsed laser excitation' and 'cryogenic crystallography with continuous-wave (CW) laser excitation', have been conducted to capture the ligand-migration pathways in native and mutant Mbs. Firstly, time-resolved crystallography is conducted with a pump–probe set-up at ambient temperature and utilizes polychromatic X-rays for Laue diffraction geometry using a stationary crystal. It enables observation of the ligand-binding dynamics at a time resolution of 100 ps by using current synchrotron radiation technology. However, the relatively higher background noise of Laue diffraction images than that of conventional monochromatic X-ray diffraction has limited the highest spatial resolution typically up to 1.8 Å, and relatively small features of the electron-density distribution tend to be smeared out in the noise level. On the other hand, the second method, cryogenic crystallography, utilizes a CW laser to produce an Mb photoproduct below glass transition temperatures. Thus, cryogenic crystallography does not access protein dynamics where thermally driven conformational fluctuations lead to rapid interconversion among conformational substates. Cryogenic crystallographic studies of Mb in combination with heat–cool cycles above and below the glass transition temperature successfully captured some intermediate states in which the CO molecule is trapped in the protein matrix (Ostermann *et al.*, 2000). However, in principle, cryogenic crystallography traps static structures of intermediate states and gives hardly any information on the time-dependent electron-density evolution. In either case, mutant Mbs which have a single mutation at the leucine 29 site (L29F, L29W and L29Q) were frequently used to stabilize the intermediate states and increase the population of them, because the population of the intermediate states in native Mb is estimated to be as low as 10%. However, the mutation causes changes in structural and electrostatic features of the internal cavities, which can eventually result in alteration of the features of the ligand-binding dynamics.

On the other hand, theoretical analysis of Mb dynamics has covered considerable new ground (Case & Karplus, 1979; Elber & Karplus, 1987). Long-timescale molecular-dynamics simulations (> 80 ns) of the migration of CO or NO inside Mb reproduced some of the previous crystallographic results (Bossa *et al.*, 2004). More recently, the gas-migration pathways inside Mb were extensively studied by the implicit ligand-sampling method (Cohen *et al.*, 2006). This method allows the location of gas-migration pathways to be assumed based on a free-energy perturbation approach, and provides complete three-dimensional maps of the potential of the mean force. The validity of these theoretical approaches needs to be evaluated experimentally.

In order to visualize the overall CO migration processes in native Mb at 1.2 Å resolution, we developed a novel cryogenic crystallographic method by using extended pulsed-laser pumping (Tomita *et al.*, 2009). The cryogenic temperature is set at 40–140 K, and the pump laser excites a carbonmonoxy myoglobin (MbCO) crystal at 15 kHz repetition rate and 4.6 mW mm^{-2} average power. This method is supposed to allow thermally driven conformational fluctuations to take place even at the cryogenic temperatures, and enables the photolyzed CO molecule to migrate with an order of several hours inside the protein matrix. In fact, we also examined experimental conditions other than the 15 kHz repetition rate trying to explore the wider energy landscape of Mb. Here we report MbCO photoproducts at 120 K using a CW laser and lasers which have 1, 10 and 15 kHz repetition rates.

2. Experimental methods

2.1. Crystallization

Sperm-whale MbCO was crystallized through several processes. Sperm-whale metmyoglobin (metMb) solution was preprocessed by flushing with CO gas with 10 m*M* Tris-HCl at pH 8.0 and minute quantities of dithionate and left for 30 min in a sealed container at 277 K. After a clear color change from brown to red, the solution was purified using a G-25 column. MbCO was crystallized at 293 K by mixing 100 µl of 6% Mb solution and 250 µl of saturated ammonium sulfate, which was also flushed with CO gas at pH 5.75. Three days later, hexagonal crystals with the monoclinic space group $P2_1$ appeared. MbCO crystals were transferred from their mother liquor to a cryoprotectant solution which consisted of the mother liquor with 15% glycerol, and then were suspended on a cryo-loop. Subsequently, the crystals were flash-cooled by a liquid-nitrogen cryogenic system and stored in liquid nitrogen until the experiment started.

2.2. Data collection and processing

The diffraction data were collected at beamline NW14A at PF-AR, KEK, using undulator U20 and a MarDTB stage with MarCCD165 detector, as shown in Fig. 2 (Nozawa *et al.*, 2007). At first, we collected a diffraction data set without laser irra-

Table 1
The excitation conditions from CW and pulsed lasers.

Repetition (kHz)	Pulse width (ns)	Average power (mW mm^{-2})	Pulse power (μJ mm^{-2})	Peak power (W mm^{-2})	Wavelength (nm)	Model number
15	2	4.6	0.31	153.3	532	ELFORLIGHT/SPOT250-1064/532
10	10	4.6	46	46	532	Laser Compact/GCL-100-S
1	1000	4.6	4.6	4.6	527	Spectra-Physics/EVOLUTION-15
CW	–	4.6	–	0.0046	532	CrystaLaser/LCS-DTL-314QT

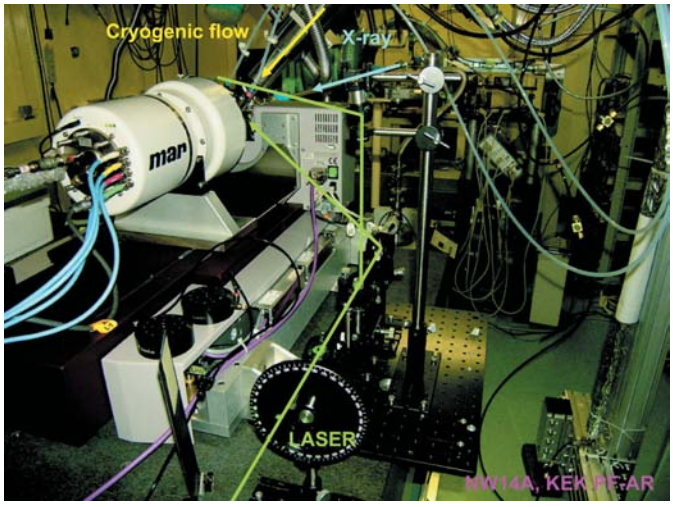

Figure 2
Experimental set-up at the beamline NW14A, Photon Factory Advanced Ring, KEK, Japan.

diation. Then, we started pulsed-laser irradiation and collected more than 30 diffraction data sets using the same crystal under repetitive pulsed-laser pumping at each temperature. Each data collection took about 30 min. Photolysis was performed using laser irradiation around 532 nm wavelength at an average power of 4.6 mW mm^{-2} (Table 1). Each MbCO crystal was illuminated from both sides of the crystal, cooled to 100–140 K by cold nitrogen gas and to 40 K by cold helium gas. The data sets were processed and scaled using the *HKL2000* program (Otwinowski & Minor, 1997). The structures were refined using *refmac* in the *CCP4* program suite 6.0.0 (Collaborative Computational Project, Number 4, 1994) using Protein Data Bank (PDB) entry 1MBC as a starting model. The cavity volumes were estimated by the *CASTp* program (Dundas *et al.*, 2006). The integrated number of electrons was calculated using the *FFT*, *MAPMASK* and *MAPDUMP* programs in the *CCP4* program suite 6.0.0.

Photodissociation of the CO molecule from the heme iron was also confirmed by the microspectrophotometry of the MbCO crystal under the same pulsed-laser pumping conditions as shown in Fig. 3. The spectral change around the visible region (500–650 nm) indicates that the CO molecule is photodissociated from the heme iron.

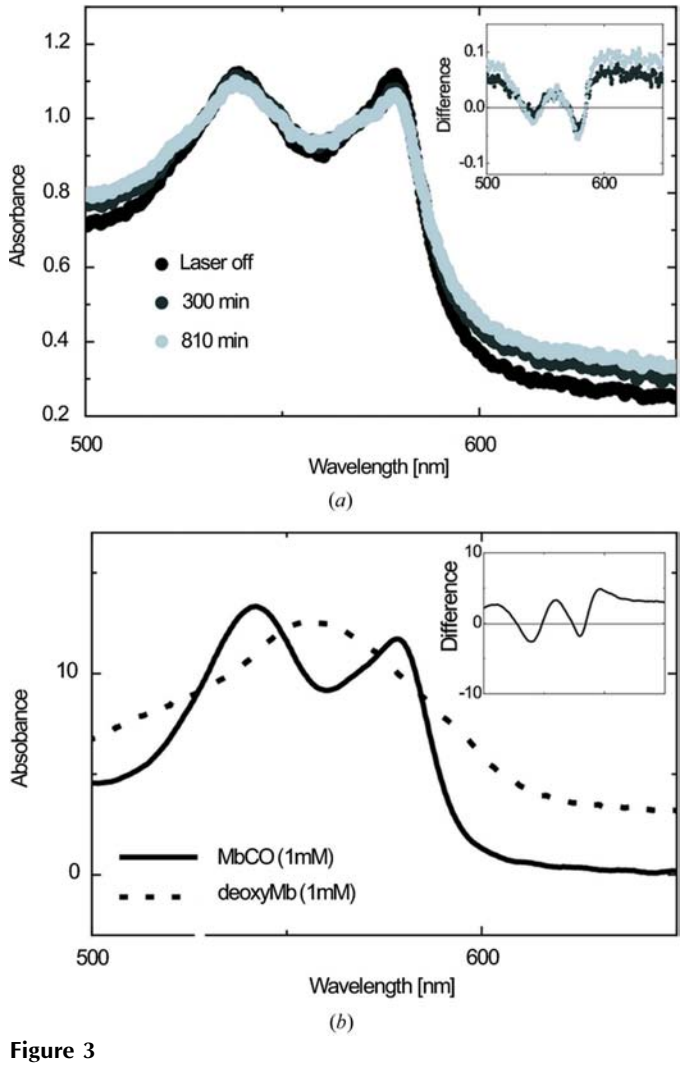

Figure 3
Visible absorption spectra (*a*) of MbCO in the crystal with pulsed-laser illumination at 15 kHz measured by microspectrophotometry at 120 K and (*b*) of MbCO and deoxy Mb in solution at ambient temperature. Inset: the differential absorption spectra against the initial MbCO spectrum.

3. Results and discussion

In order to explore the energy landscape of ligand-migration dynamics in Mb, we examined experimental conditions with various laser repetition rates and pulse durations (CW to 15 kHz) and various temperatures (40–140 K), as listed in Table 1. The average laser power density was fixed at 4.6 mW mm^{-2}.

3.1. CO migration in Mb with pulsed-laser illumination at 15 kHz repetition rate at 40–120 K

The clearest results for CO migration dynamics in Mb were obtained at a 15 kHz laser repetition rate and 2 ns pulse

Table 2
Data collection and crystallographic analysis statistics using pulsed-laser (15 kHz) illumination at 40 K and using various repetition rates and pulse durations of lasers (CW to 10 kHz) at 120 K.

	Pulsed laser (15 kHz)		CW laser		Pulsed laser (1 kHz)		Pulsed laser (10 kHz)	
	Laser off	Laser on	Laser off	810 min	Laser off	870 min	Laser off	600 min
Temperature (K)	40	40	120	120	120	120	120	120
Space group	$P12_11$	$P12_11$	$P12_11$	$P12_11$	$P12_11$	$P12_11$	$P12_11$	$P12_11$
a (Å)	34.312	34.310	34.351	34.487	34.352	34.430	34.372	34.404
b (Å)	30.618	30.630	30.631	30.634	30.586	30.601	30.608	30.618
c (Å)	63.714	63.729	63.655	63.890	63.634	63.827	63.700	63.781
β (°)	105.742	105.761	105.343	105.453	105.404	105.438	105.375	105.392
Wavelength (Å)	0.827	0.827	0.827	0.827	0.827	0.827	0.827	0.827
Resolution (Å)	50.0–1.21	50.0–1.21	50.0–1.21	50.0–1.21	50.0–1.21	50.0–1.21	50.0–1.21	50.0–1.21
R_{merge}	0.033	0.033	0.042	0.046	0.033	0.039	0.052	0.060
$I/\sigma(I)$	15.4	15.1	10.9	9.4	11.5	9.4	9.2	8.1
Completeness (%)	94.7	95.5	92.2	62.1	89.7	69.3	90.4	75.7
Redundancy	3.7	3.7	3.6	3.5	3.7	3.5	3.6	3.5
No. of reflections	37292	37319	37094	25230	36234	28073	36247	30579
R factor	0.148	0.147	0.148	0.146	0.156	0.153	0.150	0.150
R_{free}	0.186	0.180	0.188	0.185	0.193	0.213	0.194	0.193
No. of atoms	1449	1443	1445	1391	1423	1394	1433	1411
Mean B value (Å^2)	13.234	13.160	14.379	21.691	15.178	19.749	14.615	16.996
R.m.s.d. bond length (Å)	0.020	0.020	0.022	0.029	0.022	0.022	0.022	0.022
R.m.s.d. angle (°)	1.909	1.922	2.064	2.338	2.064	2.064	2.064	2.064
PDB ID	3E4N	3ECL	–	–	–	–	–	–

duration at 532 nm. Firstly, we determined the structures of MbCO and its photoproduct at 40 K (Fig. 4). As reported previously by cryogenic and time-resolved crystallographic studies, we observed the same structural features of the initial photoproduct at a slightly higher resolution (Teng *et al.*, 1994; Schlichting *et al.*, 1994; Hartmann *et al.*, 1996). The CO molecule moves to the primary docking site in the heme cavity

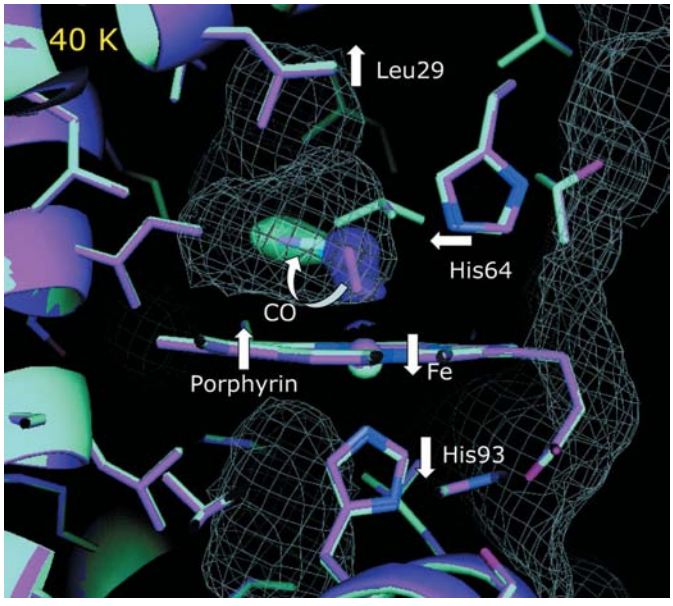

Figure 4
The crystal structures of MbCO before and after photodissociation of CO at 40 K are superimposed and shown in magenta and cyan, respectively. The molecular surface of MbCO and the surfaces of the internal cavities are shown by the mesh. The electron densities of bound and photodissociated CO molecules in the DP are represented in magenta and cyan, respectively, by using a $2F_o - F_c$ map (contoured at 0.7 e Å^{-3}). The movements of CO, the heme iron atom, His64, Leu29 and His93 after photodissociation are shown by white arrows.

around 3.74 Å from the heme Fe atom, and the Fe atom shifts by 0.26 Å out of the mean heme plane. This displacement is transmitted through His93 to the F-helix region. The porphyrin ring of the heme is pushed upwards, dragging residues Leu104, Ile107 and the G-helix to which it is attached. The data collection and crystallographic analysis statistics at 40 K are shown in Table 2. When the temperature was raised from 40 to 100–140 K, the photodissociated CO molecule in the heme cavity moves back to the iron-binding site because the internal binding rate of CO to the Fe atom overcomes the photodissociation rate at the higher temperatures. However, at the same time, the remaining photodissociated CO starts to migrate very slowly into other internal cavities, as shown in Fig. 5. As the analyzed crystal structure is the average structure of all Mb molecules in the crystal, the occupancy of the CO molecule in the cavities corresponds to the population of myoglobin molecules with particular intermediate structures, and is directly connected to the free-energy difference between the cavities. The Xe3 cavity is partially occupied by a water molecule before starting the pulsed-laser illumination. The CO migrates into a cavity in the lower part of the heme plane (Xe1 cavity) and to the back of the DP (Xe4 cavity) after 300 min laser irradiation. It is worth noting that time-resolved and cryogenic crystallography of wild-type MbCO did not capture the electron density of the CO molecule in the Xe4 cavity, probably due to the low occupancy and/or high mobility of the CO molecule in the Xe4 cavity above 120 K (Schotte *et al.*, 2004; Chu *et al.*, 2000). Instead, by using Mb mutants in which the Leu29 position is replaced by Phe, Trp or Tyr, the CO molecule was trapped in the Xe4 cavity by stabilizing the free-energy level of the Xe4 cavity (Ostermann *et al.*, 2000; Schotte *et al.*, 2003; Bourgeois *et al.*, 2003, 2006). Other features emerge at the Xe2 cavity 450 min after pulsed-laser pumping. Accumulation of the CO molecule in the Xe1 cavity was reported previously by time-resolved and cryogenic

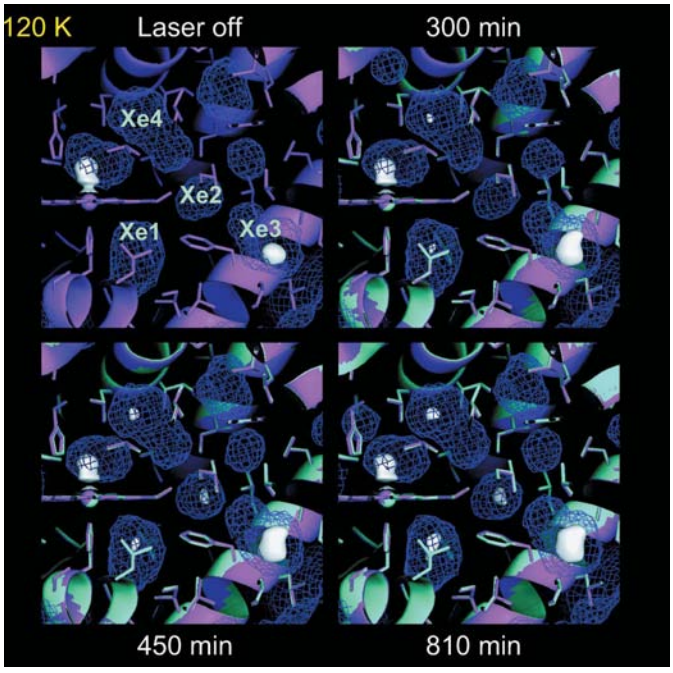

Figure 5
The crystal structures of MbCO before and after 300, 450 and 810 min laser illumination at 120 K are superimposed and shown in magenta and cyan, respectively. The molecular surface of MbCO and the surfaces of the internal cavities are shown by the mesh in purple. The electron densities of bound and photodissociated CO molecules in the DP are represented in white, by using a $2F_o - F_c$ map (contoured at 0.3 e Å^{-3}). The Xe3 cavity is partially occupied by a water molecule before starting the laser illumination.

crystallographic studies (Šrajer *et al.*, 1996; Schotte *et al.*, 2003; Schmidt *et al.*, 2005; Chu *et al.*, 2000; Ostermann *et al.*, 2000). However, regarding the Xe2 cavity, this is the first direct evidence of the time-dependent evolution of electron densities of the CO molecule, which indicates that the Xe2 cavity is involved in the CO migration channel in Mb. Table 3 summarizes the previous results from time-resolved Laue crystallography and cryogenic crystallography studies using wild-type and mutant MbCO.

Fig. 6 shows the correlation between the integrated number of electrons in each cavity and cavity volume for various illumination times for the Xe1, Xe2, Xe3 and Xe4 sites at 100, 120 and 140 K. As the CO molecule migrates into cavities, each cavity volume varies with time at each temperature. The migration of CO to the Xe4 site is dominant at 100 K, while CO starts to migrate further at 120 K, and migration to the Xe1 and Xe2 cavities becomes dominant at 140 K. The Xe3 cavity is originally occupied by a water molecule (Fig. 5), and it is probable that the increased electron density in Xe3 corresponds to a combination of the photodissociated CO molecule and the water molecule from the external solvent. Our structural analysis clearly shows that the time dependence of the electron density of the CO molecule in the Xe1, Xe2 and Xe4 cavities correlates to the change in the estimated volume of each cavity, as shown in Fig. 6. This result indicates that the CO migration in the cavity causes expansion of the cavity itself, resulting in self-opening of the channel (Fig. 7). Our novel method proposes a new view of the multiple-kinetic model, as described in Fig. 7. The migration of the CO molecule in a cavity induces the correlated expansion of the

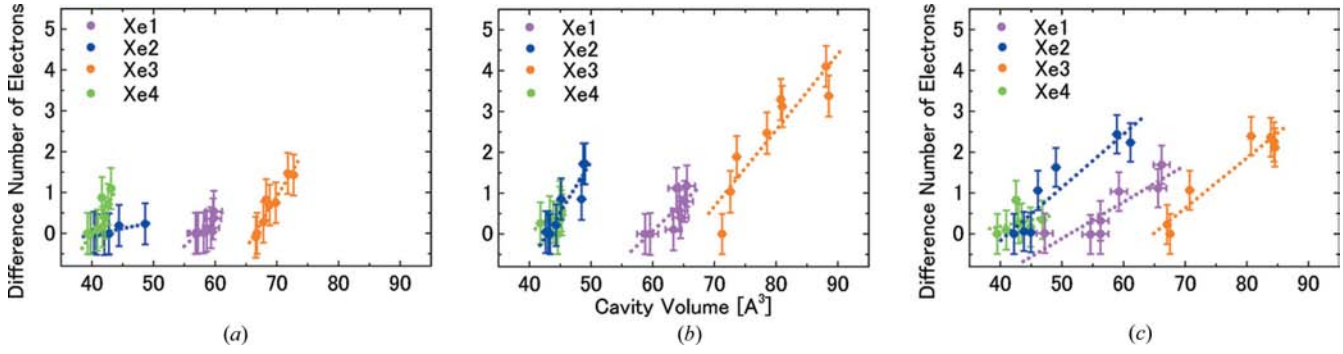

Figure 6
Correlation between the number of electrons and cavity volume for the Xe1, Xe2, Xe3 and Xe4 cavities at (*a*) 100, (*b*) 120 and (*c*) 140 K.

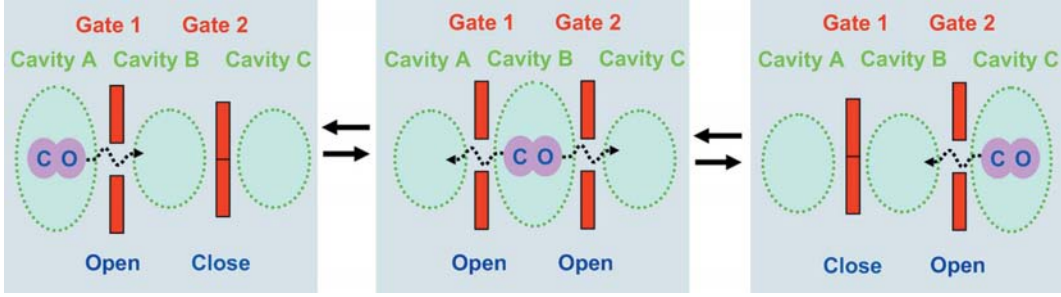

Figure 7
Schematic drawing of the cooperative ligand migration (self-opening pathway model) in a protein.

Table 3
Comparison of laser-photolysis studies with MbCO crystals.

(*a*) Polychromatic diffraction

Temperature (K)	Laser-excitation condition	Mutation†	Internal cavities where CO molecule is trapped	Reference
283	630 nm, 2.2 ns, 4–5 mJ mm^{-2}	sw L29Y, H64Q, T67R MbCO	Xe4 (3 ns), Xe1 (316 ns)	[1]
283	520–560 nm, several tens of ps, 40 µJ	sw L29Y, H64Q, T67R MbCO	Xe4 (562 ps), Xe4 (3 ns), Xe1 (316 ns)	[2]
288	615 nm, 7 ns	sw L29W MbCO	Xe1 (300 ns)	[3]
283	570 nm, 1 ps, 23 µJ, 0.88 mJ mm^{-2}, 580 nm, 2 ns, 1 mJ, 0.79 mJ mm^{-2}	sw L29F MbCO	Primary docking site (100, 316 ps), Xe4 (1, 3.16 ns), Xe1 (31.6 ns, 3.16 µs)	[4]
283	530–580 nm, ∼100 ps, 41 µJ, 1.5 mJ mm^{-2}	sw wild-type MbCO	Primary docking site (100 ps to 31.6 ns), Xe1 (316 ns)	[5]
291–293	630 nm, 7.5 ns, 1 mJ	sw wild-type MbCO	Primary docking site (4 ns)	[6]
291–293	630 nm, 7.5 ns, ∼5 mJ	sw wild-type MbCO	Primary docking site (1 ns), Xe1 (362 ns)	[7]

(*b*) Monochromatic diffraction

Temperature (K)	Laser-excitation condition	Mutation†	Internal cavities where CO molecule is trapped	Reference
22	White, fiber optics	hh MbCO	Primary docking site	[8]
88 (after 6 h illumination, 160 K)	Green, Ar^{+}-ion laser, 4.6 mW mm^{-2}		Xe1	
36	690 nm, laser diode, 20 mW/1 mm diameter	sw wild-type MbCO	Primary docking site	[9]
105	532 nm, CW, 30–200 mW	sw L29W MbCO	Xe4	[10]
105 (after illumination, 180 K)			Xe1	
20	White, fiber optics	sw wild-type MbCO	Primary docking site	[11]
40	633 nm, CW, 10 mW mm^{-2}	sw wild-type MbCO	Primary docking site	[12]
20–40	633 nm, CW, 1.7 mW/0.5 mm diameter	sw wild-type MbCO	Primary docking site	[13]
40–140	532 nm, 2 ns, 15 kHz, 4.6 mW mm^{-2}	sw wild-type MbCO	Primary docking site, Xe1, Xe2, Xe3, Xe4	[14]
120	532 nm, 10 ns, 10 kHz, 4.6 mW mm^{-2}	sw wild-type MbCO	Xe4	[15]
	527 nm, 1 ms, 1 kHz, 4.6 mW mm^{-2}	sw wild-type MbCO	Xe4	[15]
	532 nm, CW, 4.6 mW mm^{-2}	sw wild-type MbCO	Xe4	[15]

† sw Mb: myoglobin which has an amino-acid sequence based on the sequence of sperm-whale myoglobin (some sw Mb have an additional mutation, D122N, and crystallize in the space group *P*6); hh Mb: myoglobin from horse heart. References: [1] Bourgeois *et al.* (2003); [2] Bourgeois *et al.* (2006); [3] Schmidt *et al.* (2005); [4] Schotte *et al.* (2003); [5] Schotte *et al.* (2004); [6] Šrajer *et al.* (1996); [7] Šrajer *et al.* (2001); [8] Chu *et al.* (2000); [9] Hartmann *et al.* (1996); [10] Ostermann *et al.* (2000); [11] Schlichting *et al.* (1994); [12] Teng *et al.* (1994); [13] Teng *et al.* (1997); [14] Tomita *et al.* (2009); [15] this study.

cavity itself mainly due to steric interactions, which promotes the self-opening of the CO migration channel by an induced fit. The expansion of the cavity facilitates further ligand migration, as shown in Fig. 8. Here the kinetic potential barriers between the cavities are no longer defined statically but rather tuned dynamically by the ligand migration itself (Fenimore *et al.*, 2002; Austin *et al.*, 1975). This picture should be further examined by theoretical mapping the potential of the mean force (Cohen *et al.*, 2006).

Fig. 9 shows superposed structures before laser illumination (magenta) and after 750 min laser illumination (cyan) at 140 K. Yellow arrows show movements of the amino-acid residues around the DP and Xe cavities. The gating motion to open the migration pathway is evidently detected. Red arrows show movements of the amino-acid residues between internal cavities and the outer solvent area of the Mb molecule. Fig. 8

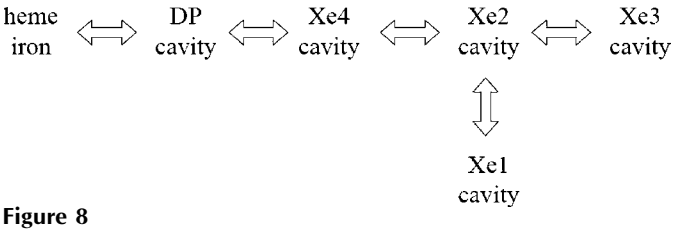

Figure 8
Ligand migration pathway in MbCO at cryogenic temperatures.

reveals the expansion of the cavities and putative gating motions of the surrounding amino-acid residues. The residues involved are as follows: Leu29, His64 and Val68 (between the DP and the Xe4 cavity), Leu69, Leu72, Ile107 and Ile111 (between the Xe4 and Xe2 cavities), Leu76, Leu135 and Phe138 (between the Xe2 and Xe3 cavities), Leu89, Leu104 and Phe138 (between the Xe2 and Xe1 cavities), and Trp7, His82 and Leu137 (between the Xe3 cavity and the solvent). The arginine 45 residue (R45) is seated between the DP and the solvent side, and a great deal of experimental evidence suggests it is the main direct gate from the DP to the solvent at ambient temperatures. We observed the gating motion of amino-acid residues (W7, L137 and H82) between the Xe3 cavity and the solvent area. Our result suggests that the route from the DP to the Xe3 cavity involving the Xe1, Xe2 and Xe4 cavities is the major ligand-migration pathway in Mb under our cryogenic conditions, as shown in Fig. 8. This scheme is basically consistent with the picture of ligand-migration channels derived from the molecular-dynamics simulation (Bossa *et al.*, 2004; Cohen *et al.*, 2006), while the implicit ligand-sampling method proposed other channels and exits (Cohen *et al.*, 2006). Although we showed that the ligand-migration pathway in Fig. 8 is the major pathway under our cryogenic conditions, other pathways shown by Cohen *et al.* (2006) or a direct pathway *via* the His64 gate at ambient

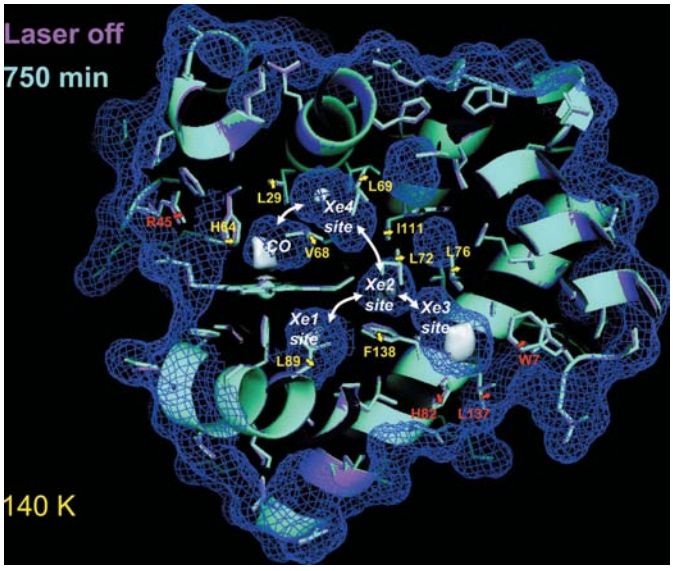

Figure 9
The crystal structures of MbCO before and after 750 min pulsed-laser illumination at 15 kHz and at 140 K are superimposed and shown in magenta and cyan, respectively. The molecular surface of MbCO and the surfaces of internal cavities are shown by the mesh in purple. The electron densities of bound and photodissociated CO molecules in the cavities are represented in white, by using a $2F_o - F_c$ map (contoured at 0.3 e Å^{-3}). The pathways of CO molecules are shown by white arrows and the displacement of inner and outer amino-acid residues are shown by yellow and red arrows, respectively.

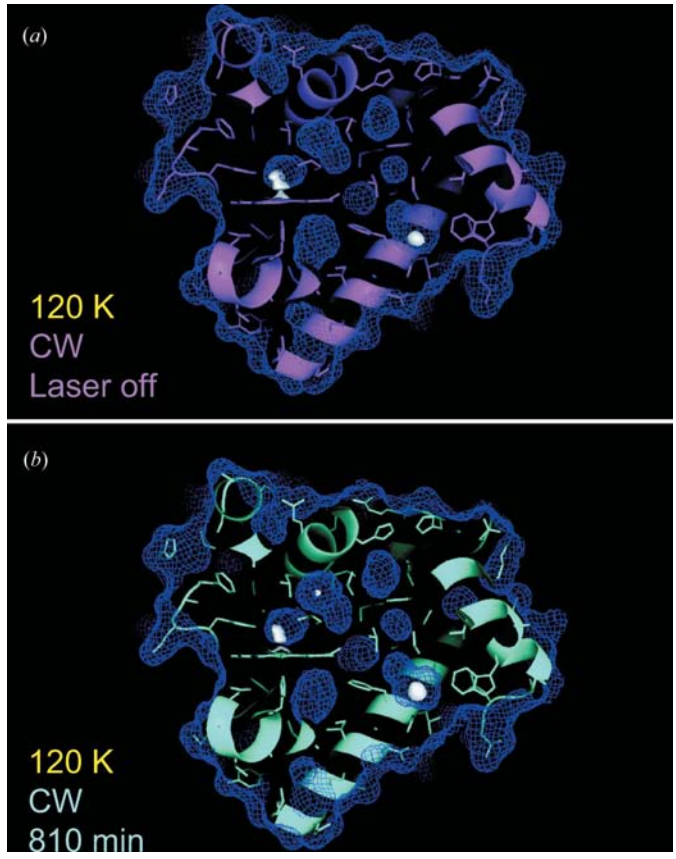

Figure 10
The crystal structures of MbCO (*a*) before and (*b*) after 810 min CW laser illumination at 120 K are shown in magenta and cyan, respectively. The molecular surface of MbCO and the surfaces of internal cavities are shown by the mesh in purple. The electron densities of the CO molecule in the cavities are represented in white, by using a $2F_o - F_c$ map (contoured at 0.3 e Å^{-3}).

temperatures are not ruled out by our result. We did not detect such channels and exits, but it might be possible to find other pathways with other temperature and/or excitation conditions.

3.2. CO migration in Mb with lower laser peak power density and repetition rate (CW, 1 and 10 kHz) at 120 K

We carried out cryogenic crystallography experiments with different types of laser illumination conditions, CW and pulsed-laser (1 and 10 kHz) illumination at 120 K. The details of the excitation conditions are summarized in Table 1, and the data collection and crystallographic analysis statistics using CW and pulsed-laser (1 and 10 kHz) illumination at 120 K are shown in Table 2. The overall features of the CO migration are basically the same in three cases; only the Xe4 cavity is occupied by a CO molecule even after several hundred minutes of laser illumination, as shown in Fig. 10. The number of electrons in the Xe4 cavity are integrated and plotted in Fig. 11(*a*). It is clearly shown that the number of electrons in the Xe4 cavity correlates with the peak power density of the laser. These results suggest the following two ideas. Firstly, the energy barrier to open the gate channels between the DP and the Xe4 cavity is comparable to the excess kinetic energy of a photodissociated CO molecule which is exerted by the laser excitation. Secondly, the repetition rate and/or the peak laser power density would be crucial parameters for inducing thermal fluctuation for CO migration in Mb even at cryogenic temperatures. If the local temperature jump exerted by the laser excitation exceeds the glass transition temperature (∼180 K), thermal fluctuation could be induced to facilitate ligand migration in Mb.

3.3. Relevance to the previous kinetic and structural studies

Frauenfelder and co-workers have shown that the ligand-binding process involves multiple intermediate states by low-temperature flash photolysis experiments (Austin *et al.*, 1975; Alben *et al.*, 1982). This multiple intermediate model is also shown by kinetic studies at room temperature (Henry *et al.*, 1983; Olson & Phillips, 1996; Scott & Gibson, 1997), which strongly motivated researchers to study the structural origin of the multiple intermediate states and the dynamic nature of molecular structures which enable the ligand migration. Although we firstly applied the extended pulsed-laser pumping method to crystallographic analysis of MbCO at a 15 kHz repetition rate under cryogenic conditions, it has been known for a long time by optical absorption, XAFS, IR and resonance Raman spectroscopy that extended illumination of Mb solution by light at cryogenic temperatures significantly affects the ligand-binding kinetics (Powers *et al.*, 1987; Ansari *et al.*, 1987; Šrajer *et al.*, 1996; Ahmed *et al.*, 1991; Nienhaus *et al.*, 1994). This effect was called the 'pumping effect', where

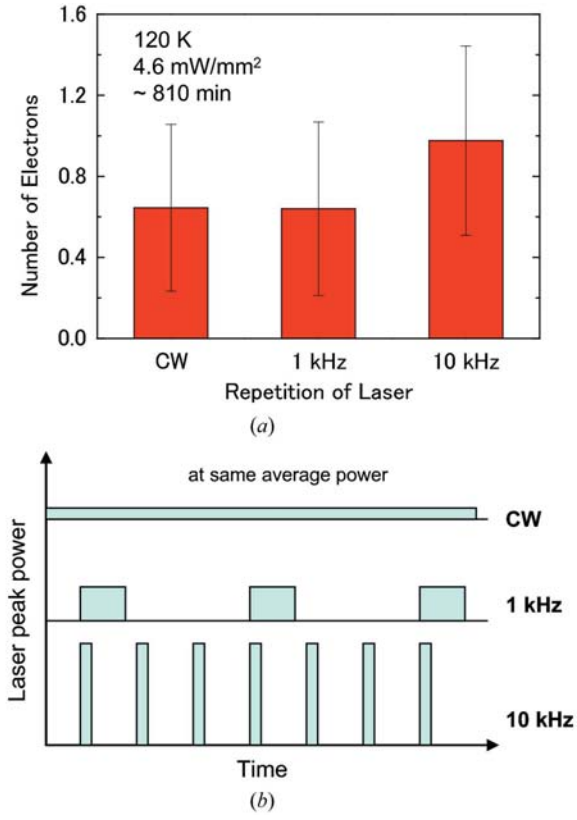

Figure 11
(*a*) The integrated number of electrons in the Xe4 cavity after laser illumination. (*b*) Schematic drawing of the peak power density and repetition rate of the pulsed lasers.

slower ligand-rebinding kinetics resulted from extended illumination. The interpretations of this observation were clustered into two groups: one group suggested that there are discrete docking sites along the ligand-binding pathway and that light pumps the system from faster to slower binding sites (Powers *et al.*, 1987; Šrajer *et al.*, 1991); the second group suggested that light modifies the protein structure, where the protein relaxes into conformational substates with slower ligand rebinding (Ansari *et al.*, 1987; Ahmed *et al.*, 1991; Nienhaus *et al.*, 1994). Our results comprehensively address the structural aspects of the 'pump effect' in Mb directly by X-ray crystallography, following the early initial work by Teng *et al.* (1997). This work provides a clear structural result that the main effect of the extended illumination at cryogenic temperatures is the slow ligand migration to more remote docking sites, while at the same time we also elucidated the interplay between ligand migration and correlated structural changes: expansion of internal cavities and opening of gates between cavities.

Terazima and co-workers applied the transient grating (TG) technique to measure the change in molecular volume of the CO escape processes in Mb, which could be qualitatively compared with our result (Sakakura *et al.*, 2001; Nishihara *et al.*, 2004). They assumed sequential and branched kinetic models similar to that shown in Fig. 8 to analyze their TG data. They estimated the molecular volume changes associated with fast (< 10 ns) and slow (∼700 ns) CO migration processes as −5 and 12 cm^3 mol^{-1}. These molecular-volume changes could be attributed to the expansion or contraction of internal cavities induced by the CO migration which have been detected in this study.

Cryogenic crystallography below 180 K detected the photolyzed CO molecule not only at the initial docking site but also in internal Xe cavities (Teng *et al.*, 1994; Schlichting *et al.*, 1994; Hartmann *et al.*, 1996; Teng *et al.*, 1997; Vitkup *et al.*, 1997; Chu *et al.*, 2000; Ostermann *et al.*, 2000). The clearest results were not obtained on the wild-type protein, but on mutant proteins, where the distal leucine 29 residue had been replaced by bulky aromatic residues such as phenylalanine and tryptophan (L29F and L29W), which artificially stabilize the reaction intermediate states. Nienhaus and co-workers detected CO molecules trapped in the Xe4 and Xe1 sites by using a cryogenic crystallographic technique in combination with heating–cooling cycles above and below the glass transition temperature (∼180 K; Ostermann *et al.*, 2000). Our method provides an alternative to cryogenic crystallography with heating–cooling cycles as proposed by Ostermann *et al.* (2000).

The time-resolved Laue-diffraction technique at ambient temperature is able to capture ligand migration through the protein matrix in real time (Šrajer *et al.*, 1996, 2001; Schotte *et al.*, 2003, 2004; Bourgeois *et al.*, 2003, 2006; Schmidt *et al.*, 2005). However, this technique is experimentally challenging and it is relatively difficult to monitor a very small fraction of intermediate states because of the relatively high background noise caused by polychromatic X-rays. Thus, complementary use of the time-resolved Laue technique and cryogenic crystallography will be favorable.

3.4. Summary and implications for general protein dynamics

Our novel method unveiled a new picture of the ligand-migration dynamics in Mb. Migration of the CO molecule in a cavity induces the structural deformation of the cavity, which promotes the opening of the gates of the CO migration channel. The structural deformation facilitates further ligand migration. We named this function a 'self-opening pathway' (Tomita *et al.*, 2009). As the gating motion is slaved by the thermal fluctuation of the protein matrix (Fenimore *et al.*, 2002), our study suggests that the ligand migration itself can modulate the equilibrium of conformational substates in physiological conditions to realize the self-opening pathway. This gating mechanism coupled with tunable thermal fluctuation by external ligand migration could explain the protein dynamics in general, and theoretical studies based on this concept will be needed in the near future.

The authors thank Kouhei Ichiyanagi, Hirohiko Ichikawa, Matthieu Chollet, Fumihiro Kawai, Sam-Yong Park, Takayuki Tsuduki and Takahisa Yamato for valuable discussions. This work was performed under the approval of the Photon Factory Program Advisory Committee (PF-PAC 2004S1-001).

References

Adachi, S., Park, S.-Y., Tame, J. R. H., Shiro, Y. & Shibayama, N. (2003). *Proc. Natl Acad. Sci. USA*, **100**, 7039–7044.

Ahmed, A. M., Campbell, B. F., Caruso, D., Chance, M. R., Chavez, M. D., Courtney, S. H., Friedman, J. M., Iben, I. E. T., Ondrias, M. R. & Yang, M. (1991). *Chem. Phys.* **158**, 329–351.

Alben, J. O., Beece, D., Bowne, S. F., Doster, W., Eisenstein, L., Frauenfelder, H., Good, D., McDonald, J. D., Marden, M. C., Moh, P. P., Reinisch, L., Reynolds, A. H., Shyamsunder, E. & Yue, K. T. (1982). *Proc. Natl Acad. Sci. USA*, **79**, 3744–3748.

Ansari, A., Berendzen, J., Braunstein, D., Cowen, B. R., Frauenfelder, H., Hong, M. K., Iben, I. E. T., Johnson, J. B., Ormos, P., Sauke, T. B., Scholl, R., Schulte, A., Steinbach, P. J., Vittitow, J. & Young, R. D. (1987). *Biophys. Chem.* **26**, 337–355.

Austin, R. H., Beeson, K. W., Eisenstein, L., Frauenfelder, H. & Gunsalus, I. C. (1975). *Biochemistry*, **14**, 5355–5373.

Bossa, C., Anselmi, M., Roccatano, D., Amadei, A., Vallone, B., Brunori, M. & Nola, A. D. (2004). *Biophys. J.* **86**, 3855–3862.

Bourgeois, D., Vallone, B., Arcovito, A., Sciara, G., Schotte, F., Anfinrud, P. & Brunori, M. (2006). *Proc. Natl Acad. Sci. USA*, **103**, 4924–4929.

Bourgeois, D., Vallone, B., Schotte, F., Arcovito, A., Miele, A. E., Sciara, G., Wulff, M., Anfinrud, P. & Brunori, M. (2003). *Proc. Natl Acad. Sci. USA*, **100**, 8704–8709.

Case, D. A. & Karplus, M. (1979). *J. Mol. Biol.* **132**, 343–368.

Chu, K., Vojtchovský, J., McMahon, B. H., Sweet, R. M., Berendzen, J. & Schlichting, I. (2000). *Nature (London)*, **403**, 921–923.

Cohen, J., Arkhipov, A., Braun, R. & Schulten, K. (2006). *Biophys. J.* **91**, 1844–1857.

Collaborative Computational Project, Number 4 (1994). *Acta Cryst.* D**50**, 760–763.

Dundas, J., Ouyang, Z., Tseng, J., Binkowski, A., Turpaz, Y. & Liang, J. (2006). *Nucleic Acids Res.* **34**, W116–W118.

Elber, R. & Karplus, M. (1987). *Science*, **235**, 318–321.

Fenimore, P. W., Frauenfelder, H., McMahon, B. H. & Parak, F. G. (2002). *Proc. Natl Acad. Sci. USA*, **99**, 16047–16051.

Hartmann, H., Zinser, S., Komninos, P., Schneider, R. T., Nienhaus, G. U. & Parak, F. (1996). *Proc. Natl Acad. Sci. USA*, **93**, 7013–7016.

Henry, E. R., Sommer, J. H., Hofrichter, J. & Eaton, W. A. (1983). *J. Mol. Biol.* **166**, 443–451.

Nienhaus, G. U., Mowant, J. R., Chu, K. & Frauenfelder, H. (1994). *Biochemistry*, **33**, 13413–13430.

Nishihara, Y., Sakakura, M., Kimura, Y. & Terazima, M. (2004). *J. Am. Chem. Soc.* **126**, 11877–11888.

Nozawa, S. *et al.* (2007). *J. Synchrotron Rad.* **14**, 313–319.

Olson, J. S. & Phillips, G. N. Jr (1996). *J. Biol. Chem.* **271**, 17593–17596.

Ostermann, A., Waschipky, R., Parak, F. G. & Nienhaus, G. U. (2000). *Nature (London)*, **404**, 205–208.

Otwinowski, Z. & Minor, W. (1997). *Methods Enzymol.* **276**, 307–326.

Powers, L., Chance, B., Chance, M., Campbell, B., Friedman, J., Khalid, S., Kumar, C., Naqui, A., Reddy, K. S. & Zhou, Y. (1987). *Biochemistry*, **26**, 4785–4796.

Sakakura, M., Morishima, I. & Terazima, M. (2001). *J. Phys. Chem. B*, **105**, 10424–10434.

Schlichting, I., Berendzen, J., Phillips, G. N. Jr & Sweet, R. M. (1994). *Nature (London)*, **371**, 808–812.

Schmidt, M., Nienhaus, K., Pahl, R., Krasselt, A., Anderson, S., Parak, F., Nienhaus, G. U. & Šrajer, V. (2005). *Proc. Natl Acad. Sci. USA*, **102**, 11704–11709.

Schotte, F., Lim, M., Jackson, T. A., Smirnov, A. V., Soman, J., Olson, J. S., Phillips, G. N. Jr, Wulff, M. & Anfinrud, P. A. (2003). *Science*, **300**, 1944–1947.

Schotte, F., Soman, J., Olson, J. S., Wulff, M. & Anfinrud, P. A. (2004). *J. Struct. Biol.* **147**, 235–246.

Scott, E. E. & Gibson, Q. H. (1997). *Biochemistry*, **36**, 11909–11917.

Šrajer, V., Reinisch, L. & Champion, P. M. (1991). *Biochemistry*, **30**, 4886–4895.

Šrajer, V., Ren, Z., Teng, T.-Y., Schmidt, M., Ursby, T., Bourgeois, D., Pradervand, C., Schildkamp, W., Wulff, M. & Moffat, K. (2001). *Biochemistry*, **40**, 13802–13815.

Šrajer, V., Teng, T.-Y., Ursby, T., Pradervand, C., Ren, Z., Adachi, S., Schildkamp, W., Bourgeois, D., Wulff, M. & Moffat, K. (1996). *Science*, **274**, 1726–1729.

Teng, T.-Y., Šrajer, V. & Moffat, K. (1994). *Nat. Struct. Biol.* **1**, 701–705.

Teng, T.-Y., Šrajer, V. & Moffat, K. (1997). *Biochemistry*, **36**, 12087–12100.

Tilton, R. F. Jr, Kuntz, I. D. Jr & Petsko, G. A. (1984). *Biochemistry*, **23**, 2849–2857.

Tomita, A., Sato, T., Ichiyanagi, K., Nozawa, S., Ichikawa, H., Chollet, M., Kawai, F., Park, S.-Y., Tsuduki, T., Yamato, T., Koshihara, S. & Adachi, S. (2009). *Proc. Natl Acad. Sci. USA*, **106**, 2612–2616.

Vitkup, D., Petsko, G. A. & Karplus, M. A. (1997). *Nat. Struct. Biol.* **4**, 202–208.